Available online at www.sciencedirect.com

SciVerse ScienceDirect

Journal of the European Ceramic Society 32 (2012) 2477–2486

www.elsevier.com/locate/jeurceramsoc

Structural and kinetic study of phase transitions in $LaYSi_2O_7$

Alberto José Fernández-Carrión [a,b], Alberto Escudero [a], Matthew R. Suchomel [c], Ana Isabel Becerro [a,*]

[a] *Instituto de Ciencia de Materiales de Sevilla (CSIC-US), c/Américo Vespucio, 49, 41092 Sevilla, Spain*
[b] *Departamento de Química Inorgánica (Universidad de Sevilla), c/Profesor García-González, 1, 41071 Sevilla, Spain*
[c] *Advanced Photon Source, Argonne National Laboratory, Argonne, IL 60439, USA*

Received 16 September 2011; received in revised form 29 February 2012; accepted 3 March 2012
Available online 30 March 2012

Abstract

Phase transitions in $LaYSi_2O_7$ have been investigated as a function of temperature using XRD, NMR and TEM. Previously described empirical crystal structure guidelines based on average cation radius in rare-earth $RE_2Si_2O_7$-type disilicates predict a stable tetragonal A-$LaYSi_2O_7$ polymorph at temperatures below 1500 °C. This study demonstrates that A-$LaYSi_2O_7$ is not thermodynamically stable at these temperatures and suggests that guidelines based on average cation size do not accurately describe the equilibrium behaviour of this silicate system. The A to G-type polymorph transition is extremely sluggish; complete transformation requires ~250 h at 1200 °C, and more than 3 weeks of calcination at 1100 °C. This observation is important when this type of material is used as environmental barrier coating (EBC) of advanced ceramics. Analysis of XRD and TEM data reveal complete substitution of Y and La on the rare-earth cation sites in both $LaYSi_2O_7$ polymorphs, but indicate preferential site occupancies in the G-type polymorph.

Keywords: Silicate; Calcination; X-ray methods; Spectroscopy; $Y_2Si_2O_7$

1. Introduction

Knowledge of the crystalline structures and phase transitions of mixed rare earth disilicates $(RE,RE')_2Si_2O_7$ is essential to understand their properties in the fields of advanced ceramics sintering and optical materials.

Rare-earth disilicates $RE_2Si_2O_7$ (RE = lanthanides, Sc and Y) are well known for their polymorphism.[1,2] They exhibit seven structure types at atmospheric pressure, known as A, B, C, D, E, F, and G, depending on the temperature and the ionic radius of the RE cation. $Y_2Si_2O_7$ shows, in addition to the B (or α), C (or β), D (or γ) and E (or δ), a low temperature form known as y-polymorph or yttrialite.[3]

Rare-earth disilicates have been extensively studied over the past several decades. Basic research studies initially focused on their unique magnetic, electrical, and optical properties, while more applied studies targeted their value as potential materials for technologically valuable applications such as microwave technology, ferromagnetics, lasers, and phosphors.[1,4] More recently, interest in these materials has been renewed by their discovery as secondary phases in sintered Si_3N_4 and SiC ceramics incorporating rare-earth oxide sintering additives. The properties of the sintered materials are strongly influenced by the type and content of their secondary phases.[5–10] Several rare-earth disilicates are also currently studied for their possible use as environmental barrier coatings (EBC) for the protection of structural ceramics in severely corrosive environments.[11–14]

Rare earth silicates also play an important role in SiAlON glasses. Pomeroy et al.[15] have demonstrated that the stability and glass properties of different SiAlON glasses doped with rare earths depend on the relative stability of the different rare earth disilicate phases that form after treatment at high temperature. Many of these applications use mixtures of different rare earth cations to improve the properties of the final material.[15–18] For example, Chen et al.[19] found that when the ratio Y_2O_3/La_2O_3 changed from 1/3 to 3/1, the predominant crystalline phase of the corresponding oxynitride glass was changed from a solid solution of $(La,Y)_5(SiO_4)_3N$ (H-phase) to a partial solid solution of $(La,Y)_2Si_2O_7$ after annealing the glasses at 1500 °C. $(La,Y)_2Si_2O_7$ (RE = La,Y) has a smaller thermal expansion

* Corresponding author. Tel.: +34 954489545; fax: +34 954460665.
E-mail address: anieto@icmse.csic.es (A.I. Becerro).

0955-2219/$ – see front matter © 2012 Elsevier Ltd. All rights reserved.
doi:10.1016/j.jeurceramsoc.2012.03.009

coefficient and higher oxidation resistance than the H-phase, so its occurrence at the grain boundaries would be of benefit for the high temperature mechanical and chemical properties of Si_3N_4 ceramics. Knowledge of the crystalline structures adopted by the $(RE,RE')_2Si_2O_7$ phases at different temperatures and RE contents is therefore of great value in understanding the behaviour and properties of these materials.

Several studies of solid solubility between disilicates of different rare earths have been reported in the literature.[3,20–29] There is clear evidence that the incorporation of rare earths of one type into the disilicate of a RE of another type has a strong influence on the stability of the different polymorphs. Pomeroy et al.[15] and Maier et al.[25] suggested and demonstrated, respectively, that the average rare-earth cation radius may be used to empirically predict phase stability in disilicate solid solutions. This so called "radius criterion" rule states that the expected polymorph for a mixed RE site silicate will be isostructural to the single RE silicate form, established by Felsche,[1] which most closely matches RE cation radius with average radius of the proposed mixed cation compound. It is noted that this concept is based on evidence from $RE_2Si_2O_7$-$RE'_2Si_2O_7$ systems that show, at least, one common polymorph.

The only structural study found in the $RE_2Si_2O_7$-$RE'_2Si_2O_7$ literature in which the end members do not show any common polymorphs is that from Monteverde and Celotti.[20] These authors studied the solid solubility of $La_2Si_2O_7$ and $Y_2Si_2O_7$ at 1600 °C, and described the structure of $(Y_{2/3}La_{1/3})_2Si_2O_7$ as isostructural with G-$La_2Si_2O_7$. However, the synthesis required an excess of amorphous silica in the initial mixture in order to obtain the desired phase. As a result, the XRD pattern of the product contained an α-cristobalite reflection four times more intense than the most intense reflection of the pursued La–Y disilicate phase, with the consequent uncertainty in the phase stability of the silicate as well as in the subsequent structure refinement.

The present study provides new information for a better understanding of the phase stabilities in the $La_2Si_2O_7$ - $Y_2Si_2O_7$ system. We have selected the 50% composition of the system ($LaYSi_2O_7$) and examined structures and phase transitions as a function of temperature, as well as conversion kinetics. The sol–gel synthetic approach used in the current study permits the formation of samples with a disilicate phase as the major product (>90 wt%). The temperature behavior of $LaYSi_2O_7$ is compared to other rare earth disilicates with RE ionic radius similar to the average rare earth radii of $LaYSi_2O_7$ to evaluate the proposed "radius criterion".

2. Experimental

2.1. Sol–gel synthesis

The $LaYSi_2O_7$ composition was synthesised following a sol–gel route. Starting reagents were $La(NO_3)_3{\cdot}6H_2O$ (99.99% Aldrich Chemical Co.), $Y(NO_3)_3{\cdot}6H_2O$ (99.99% Aldrich Chemical Co.) and $Si(OC_2H_5)_4$ (TEOS, 99% Aldrich Chemical Co.). A TEOS solution in ethanol (1:3 in volume) was added over the appropriate amounts of $La(NO_3)_3{\cdot}6H_2O$ and $Y(NO_3)_3{\cdot}6H_2O$ dissolved in 5 ml of absolute ethanol. Addition of a slight excess (10% volume) of TEOS in the initial mixture was necessary to obtain satisfactorily the $LaYSi_2O_7$ phase. This fact has also been observed by other authors[20,21,30] and does not interfere with the $LaYSi_2O_7$ behaviour because if there is any Si excess, it crystallizes as SiO_2 separated phase. The mixture was stirred at 40 °C for ~7 h and the white gel obtained was dried at 60 °C for 24 h in air. Nitrates were eliminated by calcination at 500 °C for 2 h at a heating rate of 1 °C min^{-1}.

2.2. Calcination experiments

The xerogel obtained was ground in an agate mortar and subsequently divided into different portions. They were submitted to heat treatment in air at temperatures between 1100 °C and 1650 °C and calcination times from 12 h to 21 days, with a heating rate of 5 °C min^{-1}, using a platinum crucible. Finally, the samples were slowly cooled down to room temperature.

2.3. Characterization

The global composition of the sample was examined by EDX spectroscopy with a NORAN germanium detector installed in an ATEM, Philips CM20 FEG, obtaining a Y/La molar ratio of 0.99(0.05), which agrees with the $LaYSi_2O_7$ nominal stoichiometry. EDX analyses were performed on several selected single crystals of the sample. The powdered sample was dispersed in ethanol by sonication and dropped on a conventional carbon-coated copper grid. TEM and electron diffraction were also used to study the symmetry of the different polymorphs.

Lab X-ray powder diffraction measurements were performed on a PANalytical X'Pert Pro Diffractometer (CuK_α) with an X-Celerator detector over an angular range of $10° < 2\theta < 120°$, 2θ step width of 0.02° and 10 s counting time. In addition, high-intensity and high-resolution synchrotron powder diffraction data were recorded on the 11-BM diffractometer at the Advanced Photon Source (APS), Argonne National Laboratory. The data were collected at room temperature over the 0.5–50° 2θ range, with a 0.001° step size, using a wavelength of 0.413260 Å. The sample was contained in a 0.5 mm capillary and was spun at 60 Hz during data collection.

All powder diffraction data were analysed using both Le Bail and Rietveld methods with the JANA software.[31] Refined parameters were: background coefficients, zero error, scale factors, unit cell parameters, microstructural parameters, site occupation factors for the rare earth sites, isotropic atomic displacement parameters, and atomic positions.

^{29}Si magic angle spinning nuclear magnetic resonance (MAS NMR) spectroscopy was carried out in a Bruker DRX400 Avance (9.39 T) spectrometer equipped with a multinuclear probe, using 4 mm zirconia rotors spinning at 10 kHz. A single pulse sequence was used, with an observation frequency for ^{29}Si of 79.49 MHz, a pulse width of 2.5 μs ($\pi/2$ pulse length = 7.5 μs) and a delay of 300 s. Chemical shifts are reported in ppm from tetramethylsilane (TMS). The experimental ^{29}Si NMR spectra were fitted using a modified version of the Bruker

Table 1
Polymorphs found after calcination of the xerogel with La/Y ratio = 1. A = A-$(La,Y)_2Si_2O_7$; G = G-$(La,Y)_2Si_2O_7$.

Temp (°C)	1 day	2 days	4 days	6 days	8 days	9 days	11 days
1100			A	A+G	A+G		G+A
1200	A		A+G	A+G	A+G	G+A	G
1250			G				
1300		G	G				
1500		G	G				
1600		G					

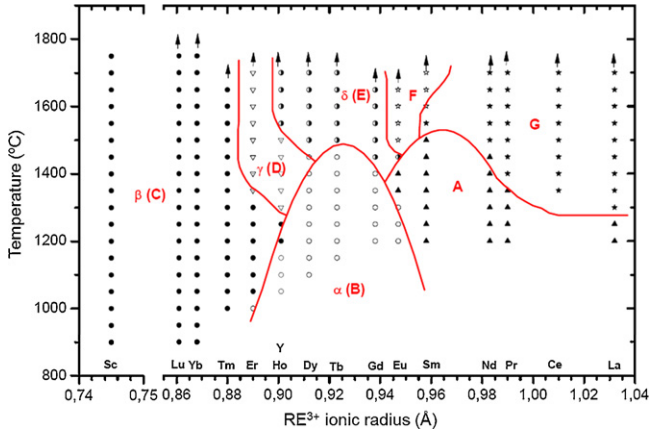

Fig. 1. Polymorphism of compounds $RE_2Si_2O_7$. After Ref. [1]. Ionic radii correspond to RE^{3+} in VI coordination.

Winfit program, which handles the finite spinning speed in MAS experiments.[32]

3. Results and discussion

3.1. Polymorph thermal stability

The average ionic radius of the two rare earth cations in $LaYSi_2O_7$ is 1.090 Å, which closely matches the Pm^{3+} ionic radius (1.093 Å).[33] However, there is no crystallographic data on $Pm_2Si_2O_7$ due to the fact that Pm is a radioactive element. More literature is available for the rare earth disilicates containing the cations Sm^{3+} and Nd^{3+}, with ionic radii just below and above Pm^{3+} (respectively 1.079 Å and 1.109 Å).[b] Following the phase diagram published by Felsche[1] (a similar diagram has been plotted here as Fig. 1), $Sm_2Si_2O_7$ exhibits the following phase transitions with temperature:

$$\underset{\text{Tetragonal } (P4_1)}{\text{A-}Sm_2Si_2O_7} \xrightarrow{1525\,^{\circ}C} \underset{\text{Monoclinic } (P2_1/c)}{\text{G-}Sm_2Si_2O_7} \xrightarrow{1575\,^{\circ}C} \underset{\text{Triclinic } (P\bar{1})}{\text{F-}Sm_2Si_2O_7}$$

On the other hand, $Nd_2Si_2O_7$ displays dimorphism, with the following polymorphs and transition temperature[1]:

$$\underset{\text{Tetragonal } (P4_1)}{\text{A-}Nd_2Si_2O_7} \xrightarrow{1475\,^{\circ}C} \underset{\text{Monoclinic } (P2_1/c)}{\text{G-}Nd_2Si_2O_7}$$

[b] The ionic radius values given correspond to the 3+ cations with coordination number VIII, as expected in most of the RE crystallographic sites of the $Sm_2Si_2O_7$ and $Nd_2Si_2O_7$ polymorphs.[1] Ionic radii have been taken from Shannon.[33]

Once formed, G-$Nd_2Si_2O_7$ is the stable phase up to the melting point of the compound. Based on the "radius criterion" explained above, $LaYSi_2O_7$ would therefore be expected to transform from a tetragonal (A-polymorph) to monoclinic (G-polymorph) symmetry in the temperature range 1475–1525 °C. At higher temperatures it could also transform into the triclinic F-polymorph, as reported for $Sm_2Si_2O_7$.

Table 1 shows, as a function of time, the polymorphs observed during the calcination of $LaYSi_2O_7$ at temperatures between 1100 °C and 1600 °C, derived from an analysis of conventional powder XRD patterns. The XRD pattern of the sample calcined at 1100 °C for 4 days matches well with PDF card 04-009-9536 (A-$La_2Si_2O_7$, tetragonal $P4_1$) with some differences in the intensity and position of the reflections. These differences are due to the different atomic form factor curves of La^{3+} and Y^{3+} as well as to the different unit cell sizes. This behaviour is in agreement with the radius criterion, since both $Sm_2Si_2O_7$ and $Nd_2Si_2O_7$ show also tetragonal symmetry at 1100 °C. Even for calcination times of up to 4 days at 1100 °C, the recorded XRD pattern is still dominated by reflections of the A-$RE_2Si_2O_7$ polymorph. However, some weak intensity reflections appear after 6 days at 1100 °C, which match the PDF 01-082-0729 (G-$La_2Si_2O_7$, monoclinic $P2_1/c$), also with slight differences in position and intensity. Further calcination time at 1100 °C promotes transformation of A- into G-$RE_2Si_2O_7$, but even 21 days are not sufficient for a complete transformation, as will be described below. The reflections are slightly shifted from those of G-$La_2Si_2O_7$ and show different intensity ratios. This indicates that a solid solution of $Y_2Si_2O_7$ in G-$La_2Si_2O_7$ is formed in these conditions.

At a higher calcination temperature of 1200 °C, the A-$RE_2Si_2O_7$ (RE = La, Y) polymorph is likewise observed for shorter calcination times <48 h, but transformation to G-$RE_2Si_2O_7$ (RE = La, Y) commences with continued calcination. Based on laboratory powder XRD analysis, complete A to G transformation is attained after 11 days at 1200 °C. The kinetics of the A to G polymorph transformation will be analysed below.

Finally, only the G-$RE_2Si_2O_7$ phase is obtained when calcination is carried out at temperatures of 1250 °C and higher, even for short calcination times. These results demonstrate that G-$RE_2Si_2O_7$ (RE = La, Y) is the stable polymorph over the studied temperature range and that $La_2Si_2O_7$–$Y_2Si_2O_7$ structural trends cannot be predicted by the radius criterion described in the Introduction section. There are two possible explanations to this fact. First, the end members of the $(La,Y)_2Si_2O_7$ system do not share any common polymorph, which is not the case of the systems used by Maier et al.[14] to demonstrate

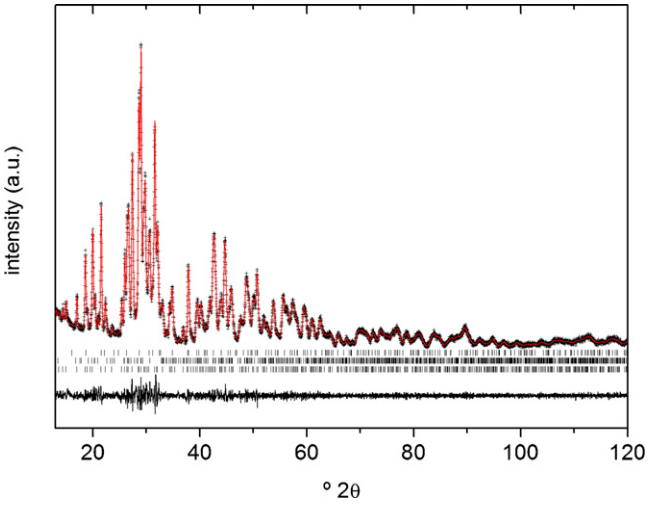

Fig. 2. Experimental (crosses) and calculated (solid line) XRD (CuK_α radiation) pattern of $LaYSi_2O_7$ annealed at 1200 °C 1 day. The difference plot is also shown. Bottom tick marks: A-$RE_2Si_2O_7$; middle tick marks: G-$RE_2Si_2O_7$; top tick marks: apatite-like silicate.

the validity of the "radius criterion" rule. Second, the "radius criterion" rule is based on the polymorphism established by Felsche[1] for single $RE_2Si_2O_7$, where RE is any lanthanide. However, although Y^{3+} shows an ionic radius very close to Ho^{3+} as well as a valence shell electronic configuration similar to lanthanides, it does not really belong to this chemical group of elements. Further studies are in progress to elucidate this question.

3.2. Study of the tetragonal A-$LaYSi_2O_7$ phase

The XRD powder pattern of the sample calcined at 1200 °C for 1 day (Fig. 2) matches the PDF 04-009-9536 corresponding to A-$La_2Si_2O_7$. All reflections appear slightly shifted with respect to the mentioned card, due to changes in unit cell dimensions and contents. The reflections are broad in general and not well resolved, indicating a low degree of crystallinity. Attempts to improve crystallization by increasing calcination time resulted in the transformation of the tetragonal to the monoclinic polymorph of $RE_2Si_2O_7$, as described above. Low intensity reflections of apatite-type phase $Y_{4.67}(SiO_4)_3O$ (PDF 04-006-9901) are also observed. Unit cell parameters for A-$(La,Y)_2Si_2O_7$, and apatite phases were refined using a LeBail fit to the XRD data (Fig. 2). Rietveld refinement was not carried out due to the low resolution of the pattern caused by the number of phases present and the broadness of the reflections. Starting unit cell parameters were taken from those reported for A-$La_2Si_2O_7$ structure[34] with space group $P4_1$ and apatite[35] with space group $P6_3/m$. Unit cell parameters obtained for A-$(La,Y)_2Si_2O_7$ were $a = 6.7664(2)$ Å and $c = 24.6868(8)$ Å, to be compared to 6.8383(7) and 24.7360(40) obtained for the A-$La_2Si_2O_7$ end-member.[34] This result indicates that smaller Y^{3+} cation enters the La^{3+} crystallographic site and decreases the resulting unit cell size.[c] TEM/EDX spectra carried out in different tetragonal single crystals confirm the presence of both cations in the crystal (Fig. 3).

3.3. Study of the monoclinic G-$LaYSi_2O_7$ phase

Synchrotron XRD has been recorded on the sample annealed at 1600 °C for 2 days to analyze the structure of the monoclinic G-$LaYSi_2O_7$ phase using the Rietveld method. Starting parameters were those described for the G-$La_2Si_2O_7$ structure[36] using space group $P2_1/c$. The La/Y ratio has been refined on each of the two rare-earth crystallographic sites present in the monoclinic cell. The global composition has been constrained to its nominal value (La/Y = 1.0). Cristobalite has been added as secondary phase (less than 8 wt%). Fig. 4 shows the experimental, fitted and difference curves. All the reflections could be fitted on the basis of a monoclinic cell with space group $P2_1/c$. Unit cell parameters obtained were $a = 5.3817(1)$ Å, $b = 8.6029(1)$ Å, $c = 14.0324(2)$ Å, and $\beta = 113.212(1)°$. Atomic parameters can be found in Table 2.

Fig. 5 shows the unit cell volume of several G-$RE_2Si_2O_7$ compounds (RE = Sm, Nd, Pr, Ce and La) as a function of the RE ionic radius, taken from Felsche.[1] The unit cell volume of the G-$LaYSi_2O_7$ phase calculated in the Rietveld fit (597.060(3) $Å^3$) has also been plotted versus the ionic radius expected from the average of the ionic radii in $LaYSi_2O_7$. This data point perfectly fits in the regression line described by the other G-$RE_2Si_2O_7$ compounds. This fact demonstrates that a solid solution of $Y_2Si_2O_7$ in G-$La_2Si_2O_7$ is formed at the 50% composition, with formation of G-$LaYSi_2O_7$. Site occupation factors of La and Y (Table 2) indicate that La occupies preferentially the rare earth crystallographic site 1 while Y is located in the rare earth site 2. Pure G-$RE_2Si_2O_7$ compounds (RE = Sm, Nd, Pr, Ce and La) show larger RE–O distances for RE site 1 compared to RE site 2. The larger ionic radius of La^{3+} compared to Y^{3+} likely drives the observed preferential cation site occupancy, as the average La1/Y1–O bond distance is greater than that of La2/Y2–O (2.568 Å vs. 2.444 Å).

Fig. 6a shows the ^{29}Si MAS NMR spectrum of the sample annealed at 1600 °C for 2 days. It consists of a unique band with a slight asymmetry towards high frequencies. The band must be composed of two Si resonances, corresponding to the two different Si crystallographic sites in the monoclinic G-$LaYSi_2O_7$ unit cell. The spectrum has been simulated with two resonances plus an additional one to fit the asymmetry observed at high frequencies. The results of the fitting are included in Table 3. The area under the curve of the resonances corresponding to Si in G-$LaYSi_2O_7$ are very similar to each other, as expected from the same occupation of both crystallographic sites in the

[c] The extremely irregular coordination polyhedra around each of the four crystallographically independent RE^{3+} cations in A-$RE_2Si_2O_7$ consist one RE atom with 7 oxygen neighbours, one with 8 and two with 9 oxygen neighbours. Ionic radii (Å) in VII, VIII, and IX coordination, respectively, are the following: Y^{3+} (0.96, 1.019, and 1.075) and La^{3+} (1.10, 1.160, and 1.216).[33]

Table 2
Refined atomic coordinates for G-$La_{1.0}Y_{1.0}Si_2O_7$ from synchrotron X-ray powder diffraction data collected at RT. Space group $P2_1/c$. $a = 5.38156(1)$ Å; $b = 8.60239(2)$ Å; $c = 14.0321(1)$ Å and $\beta = 113.212(1)^\circ$.

Atom	x	y	z	U_{iso}	Occ
La1/Y1	0.52741(7)	0.80418(3)	0.77121(2)	0.00650(8)	0.8530(15)/0.1470(15)
La2/Y2	0.85825(8)	0.60690(4)	0.59019(3)	0.00544(11)	0.1470(15)/0.8530(15)
Si1	0.7955(3)	0.24644(13)	0.02173(10)	0.0054(3)	1
Si2	0.9102(3)	0.50152(15)	0.18201(9)	0.0061(3)	1
O1	0.8513(6)	0.4215(3)	0.0711(2)	0.0152(9)	1
O2	0.0675(6)	0.1329(3)	0.0749(2)	0.0046(7)	1
O3	0.5570(6)	0.1614(3)	0.0447(2)	0.0098(8)	1
O4	0.7618(5)	0.2547(3)	0.90629(19)	0.0044(7)	1
O5	0.7413(5)	0.4251(3)	0.2419(2)	0.0025(7)	1
O6	0.2244(6)	0.4800(3)	0.2577(2)	0.0075(7)	1
O7	0.8118(5)	0.6824(3)	0.17066(19)	0.0056(7)	1

monoclinic unit cell. However, the FWHM for one site is greater, indicating a higher degree of disorder around that Si site. In fact, the Si–O distances obtained from the structure refinement described above show a higher dispersion of values at the Si1 tetrahedron compared to Si2 tetrahedron. Finally, the low intensity band at high frequency (−82.4 ppm) can be assigned to small nuclei of δ-$LaYSi_2O_7$ of insufficient domain size as to be observed by diffraction.[37]

Dupree et al.[38] reported the ^{29}Si NMR spectrum of a mixture of apatite ($La_{4.67}Si_3O_{13}$) and G-$La_2Si_2O_7$ (also referred to as h-$La_2Si_2O_7$). The spectrum consisted of two signals at −77.7 ppm and −82.6 ppm (280 Hz FWHM) that the authors assigned, respectively, to apatite and G-$La_2Si_2O_7$. The fact that a single peak is observed in spite of the two different Si crystallographic sites in G-$La_2Si_2O_7$ can likely be explained by the low resolution of their spectrum. We have synthesized apatite-free G-$La_2Si_2O_7$

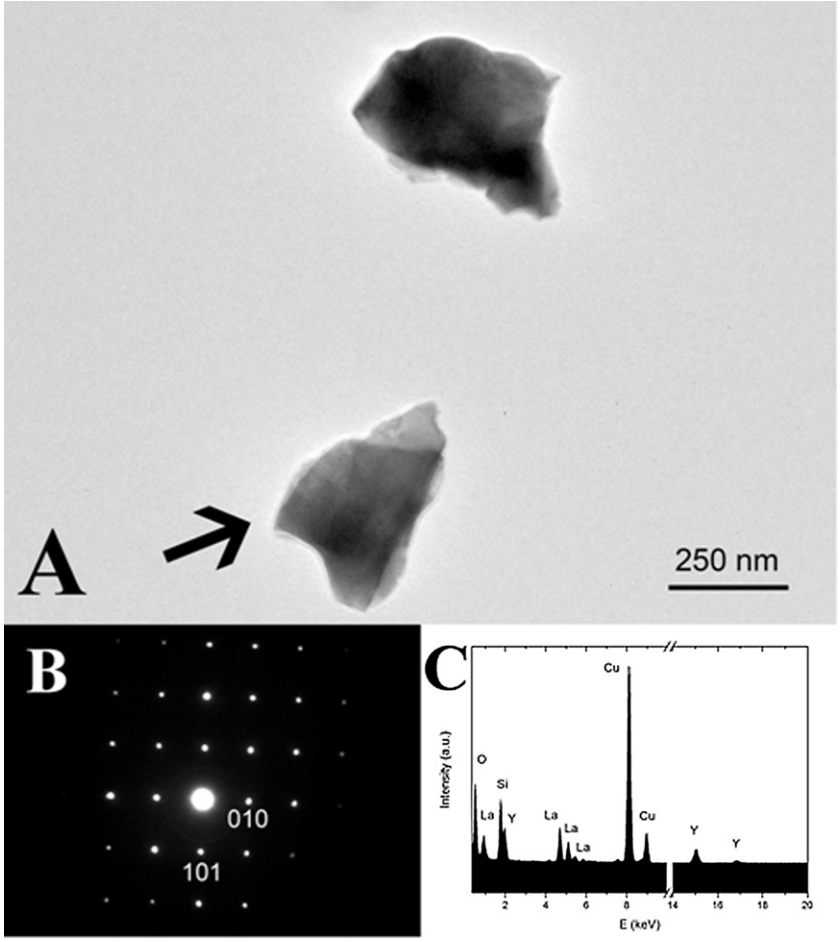

Fig. 3. (A) Bright field TEM micrograph of two $LaYSi_2O_7$ grains of the sample calcined at 1200 °C for 24 h. (B) Electron diffraction pattern of the grain marked with an arrow in A. The pattern has been indexed along the [$\bar{1}$01] zone axis of the tetragonal A-$LaYSi_2O_7$. (C) EDX corresponding to the same single crystal.

Table 3
^{29}Si MAS NMR parameters obtained from simulation of the spectra of $La_{1.0}Y_{1.0}Si_2O_7$ and $La_2Si_2O_7$ calcined at 1600 °C for 2 days.

Peak	Chemical shift (ppm)	FWHM (ppm)	Area under the curve (%)	Assignation
$La_{1.0}Y_{1.0}Si_2O_7$				
1	−86.0	2.1	45	G-$La_{1.0}Y_{1.0}Si_2O_7$
2	−84.5	2.4	46	G-$La_{1.0}Y_{1.0}Si_2O_7$
3	−82.3	1.6	9	δ-$La_{1.0}Y_{1.0}Si_2O_7$
$La_2Si_2O_7$				
1	−83.8	1.2	45	G-$La_2Si_2O_7$
2	−82.7	1.2	46	G-$La_2Si_2O_7$
3	−81.7	0.9	9	Si in another phase

following the same procedure described above for G-$LaYSi_2O_7$. The ^{29}Si MAS-NMR spectrum is shown in Fig. 6b. It shows a band with two maxima at −83.8 ppm and −82.7 ppm and FWHM values of 95 Hz each, corresponding to the two Si sites in the monoclinic unit cell of G-$La_2Si_2O_7$. The third contribution (9% of the total area) at −81.7 ppm corresponds to Si in a structure that is not detected by XRD. Comparing the ^{29}Si chemical shift values of G-$La_2Si_2O_7$ with those of G-$LaYSi_2O_7$ (Table 3) it can be observed that introducing Y in the La site shifts the signals towards lower frequency values. This fact has been assigned to differences in electronegativity of the rare earth cations in the second coordination shell of Si.[23,27,39] Finally, introducing Y in the La sites creates a high

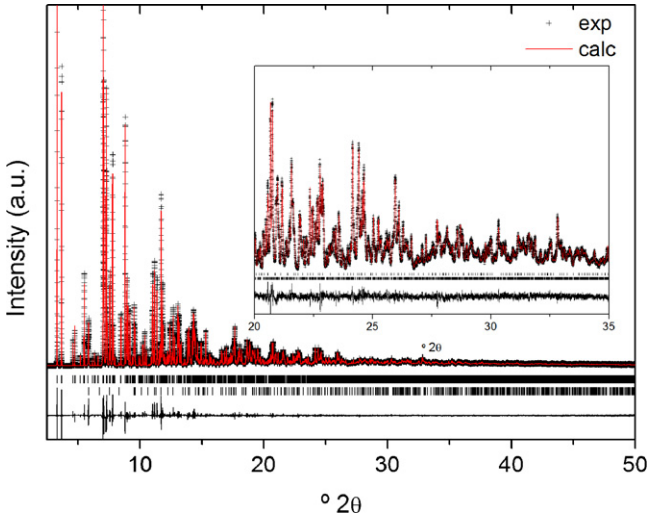

Fig. 4. Experimental (crosses) and calculated (solid line) XRD pattern (11BM synchrotron radiation) of $LaYSi_2O_7$ annealed at 1600 °C for 2 days. The difference plot is also shown. Bottom tick marks: G-$RE_2Si_2O_7$, top tick marks: cristobalite.

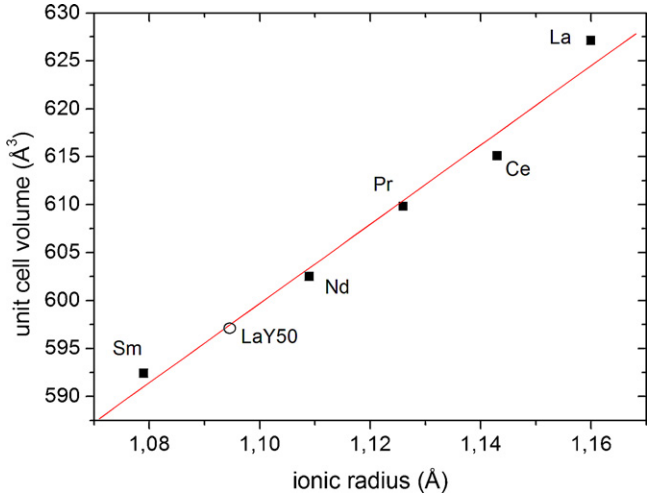

Fig. 5. Solid circles: unit cell volume of different G-$RE_2Si_2O_7$ compounds (RE = Sm, Nd, Pr, Ce and La) versus the ionic radius of the RE^{3+} with VIII coordination. Open circle: unit cell volume of G-$LaYSi_2O_7$ calculated by Rietveld fit of the corresponding XRD pattern.

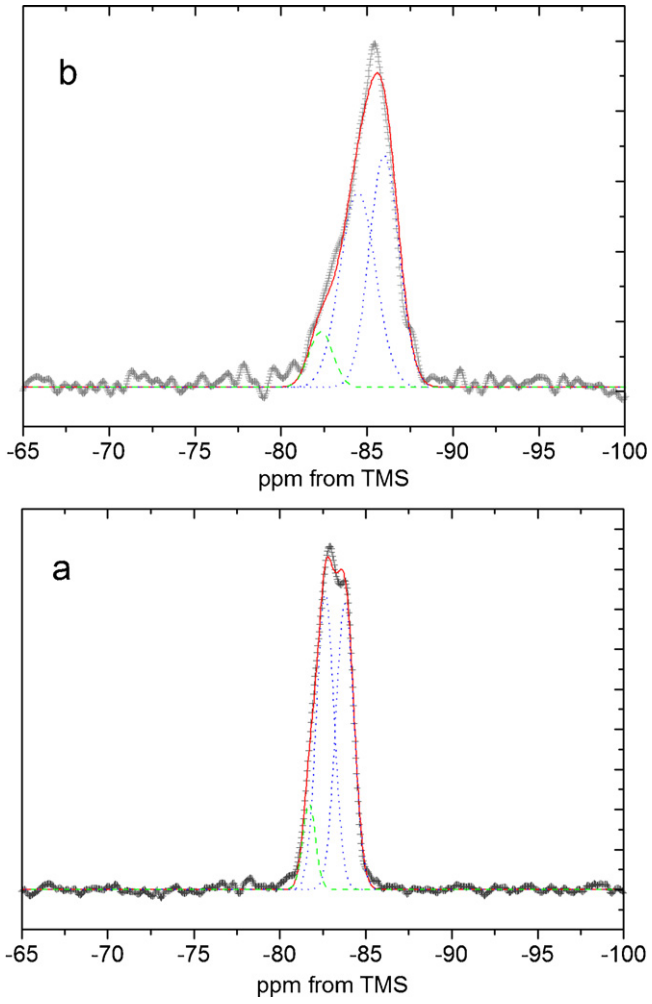

Fig. 6. Experimental (crosses) and calculated (solid line) ^{29}Si MAS NMR spectra of (a) $LaYSi_2O_7$ annealed at 1600 °C for 2 days and (b) G-$La_2Si_2O_7$. Individual contributions appear as discontinuous lines.

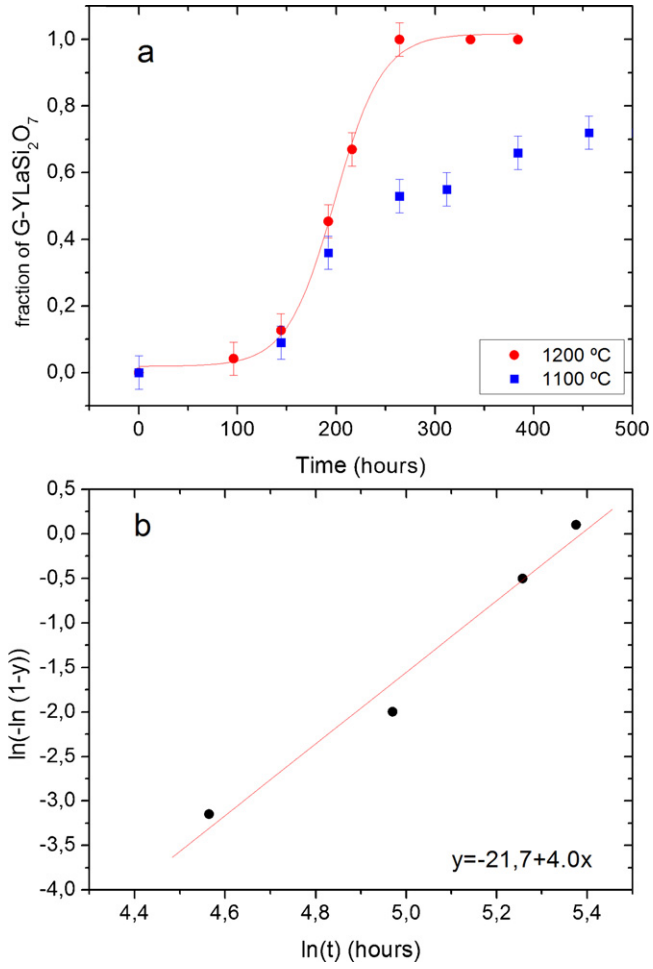

Fig. 7. (a) Fraction of G-$LaYSi_2O_7$ versus calcination time at 1200 °C (circles) and 1100 °C (squares). (b) Plot of $\ln(-\ln(1-y))$ against $\ln t$ for the transformation of A-$LaYSi_2O_7$ in G-$LaYSi_2O_7$.

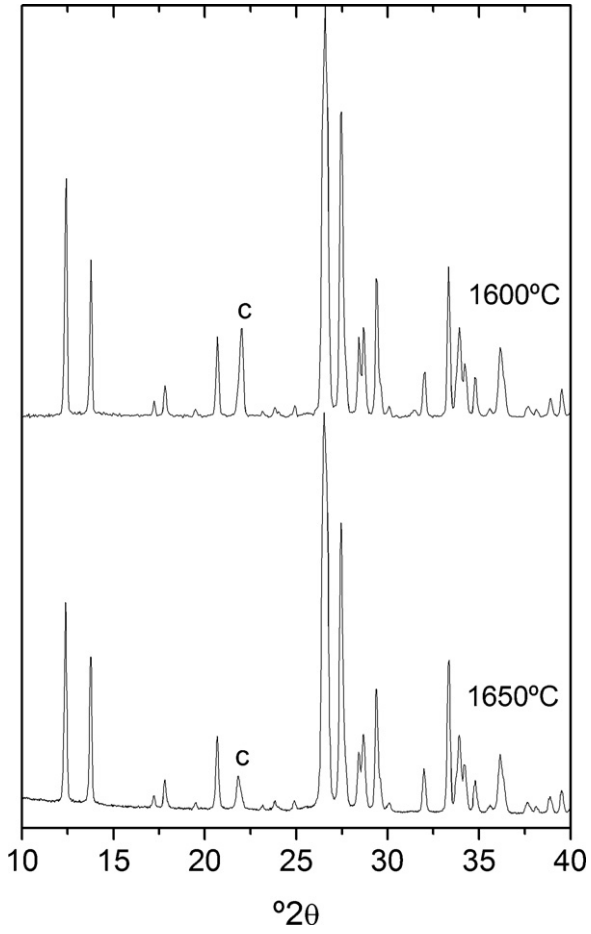

Fig. 8. XRD patterns (CuK_α radiation) of $LaYSi_2O_7$ annealed at (a) 1600 °C and (b) 1650 °C. c = cristobalite.

degree of local disorder around the Si atoms, as inferred from the differences in FWHM values between G-$La_2Si_2O_7$ and G-$LaYSi_2O_7$ (Table 3). This behaviour has also been observed in related systems such as $Lu_2Si_2O_7$-$Y_2Si_2O_7$[22] and $Sc_2Si_2O_7$-$Y_2Si_2O_7$.[26]

3.4. Transformation kinetics of A- to G-$LaYSi_2O_7$

The A-$RE_2Si_2O_7$ to G-$RE_2Si_2O_7$ phase transition is a reconstructive type transition according to the differential thermal analysis data of Felsche[1] for pure $RE_2Si_2O_7$ compounds. Reconstructive transitions involve a reorganization of the crystal structure that is achieved by breaking and reforming coordination bonds. These transitions typically have large activation energies and are kinetically very sluggish. Felsche[1] observed large variations in time, from 30 min to ∞, for the individual transitions in pure $RE_2Si_2O_7$ compounds. "∞" means no or incomplete conversion within a reasonable period of time (i.e. 100 h). The low diffusion rate of the ions involved in the "reconstructive transitions" sometimes resulted in the coexistence of two corresponding modifications. To the best of our knowledge, no kinetic study of these types of disilicate transformations has been published to date.

Fig. 7a plots the fraction of G-$LaYSi_2O_7$ versus calcination time at 1100 °C and 1200 °C. Quantification has been obtained from the Rietveld analysis of the XRD patterns. The sluggishness of the reaction can be inferred from these data, which indicate that the phase transition needs ca. 250 h to be completed at 1200 °C, while complete transformation was not observed even after 21 days (500 h) of calcination at 1100 °C. This is in good agreement with the observations of Felsche.[1] The plot at 1200 °C clearly shows a sigmoidal form, with a slower initial reaction rate, increasing with time, until plateauing as the reaction goes to completion. It is well known that the isothermal kinetics of a wide range of mineral reactions, which include reconstructive polymorphic transformations, can be described by an Avrami equation of the type:

$$y = 1 - \exp(-kt)^n \quad (1)$$

where y is the fraction transformed, k is a rate constant and n is a constant that depends on the reaction mechanism. To extract values of the rate constant k from Eq. (1), the usual approach is to linearize the equation to get

$$\ln(-\ln(1-y) = n\ \ln\ k + n\ \ln\ t \quad (2)$$

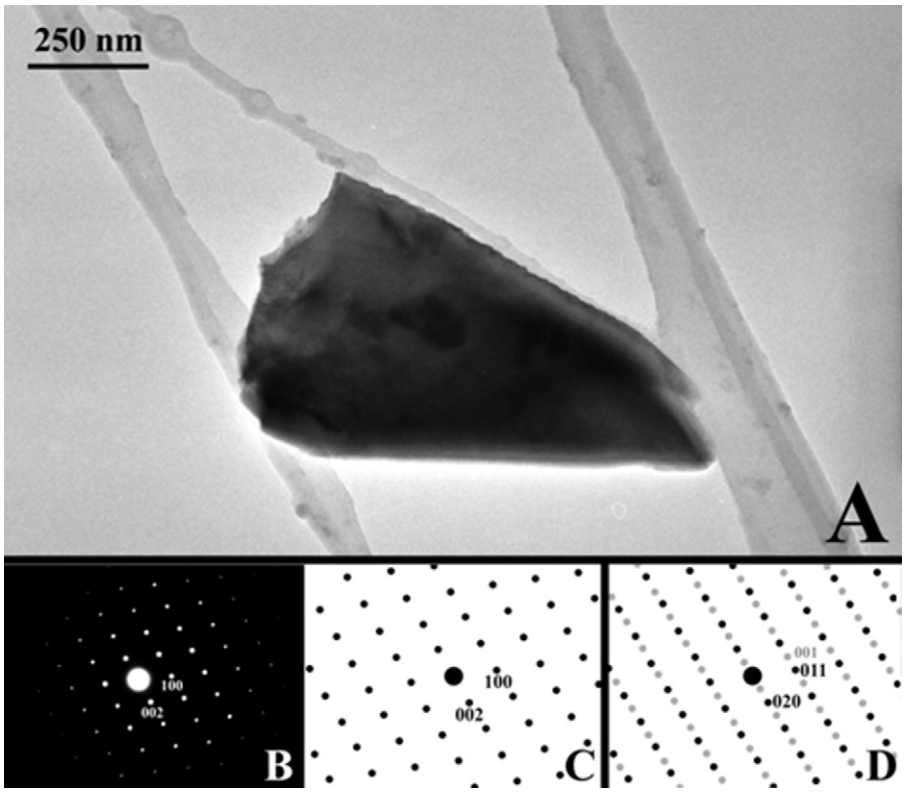

Fig. 9. (A) Bright field TEM micrograph of a $LaYSi_2O_7$ grain of the sample calcined at 1650 °C. (B) Electron diffraction pattern of the grain presented in A. The pattern has been indexed along the [0 1 0] of the monoclinic G-$LaYSi_2O_7$ phase. (C) Simulation of the electron diffraction pattern along the [0 1 0] of the monoclinic G-$LaYSi_2O_7$. (D) Simulation of the electron diffraction pattern along the [1 0 0] of the possible triclinic F-$LaYSi_2O_7$. Spots in grey correspond to the (0 0 1) and (1 0 0) family of planes that do not appear on the pattern shown in C.

Thus, a reaction whose kinetics conform to this Avrami equation gives a straight line when $\ln(-\ln(1-y))$ is plotted against $\ln t$. Fig. 7b shows the data for the A- to G-$LaYSi_2O_7$ transformation against $\ln t$ at 1200 °C. Values for n and k were $n = 4$ and $k = 4.4 \times 10^{-3}\ h^{-1}$. The physical interpretation of the Avrami constants, k and n, is not straightforward and it is still open to interpretation. According to the original theory, n should be an integer from 1 to 4, the value of which should depend only on the type of the statistical model; however, it has become customary to regard it as an adjustable parameter that may be non-integral. The value of 4 can be interpreted as nuclei non-preformed and growing at a constant nucleation rate in the three dimensions.[40] The incomplete transformation with calcination at 1100 C was too slow to be well described by the Avrami equation; higher calcination temperatures at 1250 °C and above yielded the G-$LaYSi_2O_7$ polymorph directly.

3.5. Evidence for F-$LaYSi_2O_7$ formation at higher temperatures?

As discussed above, it has been reported that G-$Sm_2Si_2O_7$ transforms to F-$Sm_2Si_2O_7$ (P-1 space group) at 1575 °C, while G-$Nd_2Si_2O_7$ is the stable polymorph up to the melting point of that composition.[1] G- and F-$RE_2Si_2O_7$ are extremely similar and difficult to distinguish by powder X-ray diffraction. In order to check whether G-$LaYSi_2O_7$ transforms into F-$LaYSi_2O_7$ or not, a sample of G-$LaYSi_2O_7$ was calcined at 1650 °C for 12 h. The XRD pattern was very similar to that of the sample annealed at 1600 °C (Fig. 8). A good fit to the powder XRD data could be obtained using both monoclinic and triclinic models, thus hindering the determination of this possible phase transition. These structures can however be distinguished by selected area electron diffraction patterns. Fig. 9A shows a silicate grain of the sample calcined at 1650 °C with its corresponding electron diffraction pattern (Fig. 9B). Similarly inconclusive, electron diffraction patterns of the different silicate grains could be indexed with both the monoclinic and triclinic symmetry. However, the electron diffraction pattern taken along the [0 1 0] zone axis considering the monoclinic structure can be distinguished from its analogous pattern taken along the [1 0 0] zone axis if the triclinic structure is considered. Both simulations are shown in Fig. 9C and D, respectively. It can be observed that the (0 0 1) and (1 0 0) families of planes appear on the electron diffraction pattern of the triclinic structure (Fig. 9D) but the analogous spots do not appear on the pattern when the monoclinic symmetry is considered (Fig. 9C). The experimental pattern presented in Fig. 9B is compatible with the one corresponding to the monoclinic symmetry. This demonstrates that $LaYSi_2O_7$ keeps the monoclinic structure of the G polymorph and does not transform into the F polymorph, at least at $T \leq 1650$ °C. The fact that $Sm_2Si_2O_7$ displays three different polymorphs with temperature reflects the rather unstable $4f^5$ electronic configuration of the Sm^{3+} cation.[1]

On the contrary, the stability of the La^{3+} ($4f^0$) and Y^{3+} ($3d^{10}$) electronic configurations favours the existence of only one stable polymorph in $LaYSi_2O_7$, in spite of the similar value of the average ionic radius of the rare earths in this compound compared to the ionic radius of Sm^{3+}.

4. Conclusions

Y enters the La sites in both A-$(La,Y)_2Si_2O_7$ and G-$(La,Y)_2Si_2O_7$ structures forming solid solutions. A-$(La,Y)_2Si_2O_7$ is not a thermodynamically stable phase and the "radius criterion" is not obeyed in this rare earth disilicate system. La occupies preferentially the rare earth crystallographic site 1 while Y is located in the rare earth site 2 in the G-$(La,Y)_2Si_2O_7$ structure. The incorporation of Y creates a high degree of local disorder around the Si atoms. The A- to G-$LaYSi_2O_7$ phase transition is extremely sluggish. It needs ca. 250 h to be completed at 1200 °C, while complete transformation was not observed after 21 days calcination at 1100 °C. Transformation of G- to F-$(La,Y)_2Si_2O_7$ at high temperature (1650 °C) was not observed in this composition. This observation is important when this type of material is used as environmental barrier coating (EBC) of advanced ceramics because of the different unit cell volumes of the polymorphs.

Acknowledgements

A.J. Fernández-Carrión gratefully acknowledges an F.P.D.I. grant from Junta de Andalucía. Supported by DGICYT (Project no. CTQ2010-14874/BQU) and Junta de Andalucía (FQM-6090). Use of the Advanced Photon Source at Argonne National Laboratory was supported by the U. S. Department of Energy, Office of Science, Office of Basic Energy Sciences, under Contract No. DE-AC02-06CH11357.

References

1. Felsche J. Polymorphism and crystal data of rare-earth disilicates of type $RE_2Si_2O_7$. *J Less-Common-Metals* 1970;**21**:1.
2. Felsche J. The crystal chemistry of the rare-earth silicates. *Struct Bond* 1973;**13**:99.
3. Ito J, Johnson H. Synthesis and study of yttrialite. *Am Mineral* 1968;**53**:1940.
4. Liddell K, Thompson DP. X-ray diffraction data for yttrium silicates. *Br Ceram Trans* 1986;**85**:17.
5. Cinibulk MK, Thomas G, Johnson SM. Oxidation behaviour of rare-earth disilicate silicon nitride ceramics. *J Am Ceram Soc* 1992;**75**:2044.
6. Kumar S, Drummond CH. Crystallization of various compositions in the Y_2O_3–SiO_2 system. *J Mater Res* 1992;**7**:997.
7. Choi HJ, Lee JG, Kim YW. Oxidation behavior of hot-pressed Si_3N_4 with Re_2O_3 (Re = Y, Yb, Er, La). *J Eur Ceram Soc* 1999;**19**:2757.
8. Klemm H. Corrosion of silicon nitride materials in gas turbine environment. *J Eur Ceram Soc* 2002;**22**:2735.
9. Matovic B, Rixecker G, Aldinger F. Pressureless sintering of silicon nitride with lithia and yttria. *J Eur Ceram Soc* 2004;**24**:3395.
10. Lojanova S, Tatarko P, Chlup Z, Hnatko M, Dusza J, Lences Z, et al. Rare-earth element doped Si_3N_4/SiC micro/nano-composites-RT and HT mechanical properties. *J Eur Ceram Soc* 2010;**30**:1931.
11. Aparicio M, Duran A. Yttrium silicate coatings for oxidation of carbon–silicon carbide composites. *J Am Ceram Soc* 2000;**83**:1351.
12. Lee KN, Fox DS, Bansal NP. Rare earth silicate environmental barrier for coating SiC/SiC composites and Si_3N_4 ceramics. *J Eur Ceram Soc* 2005;**25**:1705.
13. Suetsuna T, Ohji T. Oxidation of silicon nitride in wet air and effect of lutetium disilicate coating. *J Am Ceram Soc* 2005;**88**:1139.
14. Maier N, Nickel KG, Rixecker G. High temperature water vapour corrosion of rare earth disilicates $(Y,Yb,Lu)_2Si_2O_7$ in the presence of $Al(OH)_3$ impurities. *J Eur Ceram Soc* 2007;**27**:2705.
15. Pomeroy MJ, Nestor E, Ramesh R, Hampshire S. Properties and crystallization of rare earth Si–Al–O–N glasses containing mixed trivalent modifiers. *J Am Ceram Soc* 2005;**88**:875.
16. Hirosaki N, Okada A, Matoba K. Sintering of Si_3N_4 with the addition of rare earth oxides. *J Am Ceram Soc* 1988;**71**:C–C144.
17. Hirosaki N, Okada A. Effect of additive oxide amount on gas pressure sintering of silicon nitride. *J Mater Sci* 1992;**27**:3743.
18. Marchi J, Chaves Guedes e Silva C, Batista Silva B, Bressiani JC, de Almeida Bressiani AH. Influence of additive system (Al_2O_3–RE_2O_3, RE = Y, La, Nd, Dy Yb) on microstructure and mechanical properties of silicon nitride-based ceramics. *Mater Res* 2009;**12**:145.
19. Chen J, Wei P, Huang YJ. Formation and properties of La–Y–Si–O–N oxynitride glasses. *Mater Sci Lett* 1997;**16**:1486.
20. Monteverde F, Celotti G. Structural data from X-ray powder diffraction of a new phase formed in the Si_3N_4–La_2O_3–Y_2O_3 system after oxidation in air. *J Eur Ceram Soc* 1999;**19**:2021.
21. Monteverde F, Celotti G. Structural data from X-ray powder diffraction for new high-temperature phases $(Y_{1-x}Ln_x)_2Si_2O_7$ with Ln = Ce, Pr, Nd. *J Eur Ceram Soc* 2002;**22**:721.
22. Becerro AI, Escudero A. Phase transitions in Lu-doped $Y_2Si_2O_7$ at high temperatures. *Chem Mater* 2005;**17**:112.
23. Becerro AI, Escudero A. XRD and MAS NMR spectroscopy across the $Lu_2Si_2O_7$–$Y_2Si_2O_7$ solid solution. *J Solid State Chem* 2005;**178**:1.
24. Becerro AI, Escudero A. Polymorphism in the $Lu_{2-x}Y_xSi_2O_7$ system at high temperatures. *J Eur Ceram Soc* 2006;**26**:2293.
25. Maier N, Rixecker G, Nickel KG. Formation and stability of Gd, Y, Yb and Lu disilicates and their solid solutions. *J Solid State Chem* 2006;**179**:1630.
26. Escudero A, Alba MD, Becerro AI. Polymorphism in the $Sc_2Si_2O_7$–$Y_2Si_2O_7$ system. *J Solid State Chem* 2007;**180**:1436.
27. Ohashi H, Alba MD, Escudero A, Becerro AI. Structural study of the $Lu_2Si_2O_7$–$Sc_2Si_2O_7$ system. *J Phys Chem Solids* 2007;**68**:464.
28. Allix M, Alba MD, Florian P, Fernández-Carrión AJ, Suchomel MR, Escudero A, et al. Structural elucidation of beta-$(Y,Sc)_2Si_2O_7$: combined use of ^{89}Y MAS NMR and powder diffraction. *J Appl Cryst* 2011;**44**:846–52.
29. Fernández-Carrión AF, Escudero A, Alba MD, Becerro AI. Solid solubility of $Yb_2Si_2O_7$ in β, γ and δ-$Y_2Si_2O_7$. *J Solid State Chem* 2011;**184**:1882.
30. Boakye EE, Mogilevsky P, Hay RS, Cinibulk MK. Rare-earth disilicates as oxidation-resistant fiber coatings for silicon carbide ceramic–matrix composites. *J Am Ceram Soc* 2011;**94**:1716.
31. Petricek V, Dusek M, Palatinus L. Jana2006.The Crystallographic Computing System, Institute of Physics, Prague, Czech Republic, 2006. http://www-xray.fzu.cz/jana/jana.html.
32. Massiot D, Fayon F, Capron M, King I, Le Calvé S, Alonso B, et al. Modelling one- and two-dimensional solid state NMR spectra. *Magn Reson Chem* 2002;**40**:70.
33. Shannon RD. Revised effective ionic radii and systematic studies of interatomic distances in halides and chaleogenides. *Acta Crystallogr A* 1976;**32**:751.
34. Müller-Bunz H, Schleid T. Über den H- und A-Typ von $La_2(Si_2O_7)$. *Z Anorg Allg Chem* 2000;**626**:2549.
35. Maksimov BA, Litvin BN, Iliukhin VV, Belov NV. Hydrothermal crystallization in system A_2O–TR_2O_2–H_2O: synthesis of crystals of alkali metal yttrium silicates. *Sov Phys Crystallogr (Engl Transl)* 1969;**14**:407.
36. Christensen AN. Investigation by the use of profile refinement of neutron powder diffraction data of the geometry of the $[Si_2O_7]_6$-ions in the high temperature phases of rare earth disilicates prepared from the melt in crucible-free synthesis. *Z Kristallogr* 1994;**209**:7.

37. Parmentier J, Bodart PR, Audoin L, Massouras G, Thompson DP, Harris RK, et al. Phase transformations in gel-derived and mixed-powder-derived yttrium disilicate, $Y_2Si_2O_7$, by X-ray diffraction and Si-29 MAS NMR. *J Solid State Chem* 2000;**149**:16.
38. Dupree R, Lewis MH, Smith ME. A high-resolution NMR study of the La–Si–Al–O–N system. *J Am Chem Soc* 1989;**111**:5125.
39. Janes N, Oldfield E. Prediction of Si-29 nuclear magnetic resonance chemical shifts using a group electronegativity approach. Applications to silicate and aluminosilicate structures. *J Am Chem Soc* 1985;**107**: 6769.
40. Jena AK, Chaturvedi MC. *Phase transformations in materials*. Prentice Hall; 1992. p. 243–247.